VORTEX FLOW MANIPULATION ON GENERIC DELTA WING CONFIGURATIONS

Anja Kölzsch*, Christian Breitsamter*
***Institute for Aerodynamics and Fluid Mechanics, Technische Universität München**
Anja.Koelzsch@aer.mw.tum.de; Christian.Breitsamter@aer.mw.tum.de

Keywords: *Aerodynamics, Vortex Flow Control, Wind Tunnel Testing*

Abstract

The manipulation of characteristic vortex flow instabilities, which occur in the flow around delta wings, is of great interest for increasing the performance of such configurations. This work presents experimental results of vortex flow manipulation on generic delta wing configurations using pulsed blowing slot actuators along the leading edge. The frequencies of the examined blowing cases are chosen on the basis of unsteady characteristics which occur in the shear layer roll-up during vortex formation and vortex breakdown, respectively.
The results of hot-wire measurements substantiate the receptivity of the shear layer for the pulsed excitation until into the vortex core. The flowfield response to this periodic forcing is shown by the displacement of the vortex bursting location in a chord-wise direction, thus satisfying the aim of enhancing the aerodynamic performance.

Nomenclature

b	wing span [m]
C_μ	momentum coefficient [-]
c_r	root chord [m]
f_{pulse}	pulse frequency [Hz]
h	slot length [m]
$\dot{m}$	mass flow [kg/s]
Re_{mac}	Reynolds number based on mean aerodynamic chord [-]
s	wing half span [m]
S	spectral density of velocity fluctuations [$m^2/s^2 \cdot 1/Hz$]
t	slot width [m]
u, v, w	axial, lateral and vertical velocity in wind-tunnel fixed system [m/s]
$u_{rms}, v_{rms}, w_{rms}$	rms values of u', v', w' [m/s]; $u_{rms} = \sqrt{\overline{u'^2}}$
U_∞	free-stream velocity [m/s]
Y, Z	wing coordinates related to local half span, i.e. $Y = y/s_l$ [-]
α	angle of attack [°]
ρ	density [kg/m^3]
φ	leading-edge sweep [°]
Λ	aspect ratio [-]
CTA	Constant Temperature Anemometry
HWA	Hot-Wire Anemometry
PSD	Power Spectral Density
VFE	Vortex Flow Experiment
Indices	
b	coordinates in body-fixed system
l	local wing coordinate

1 Introduction

The flow around wing configurations of high sweep and modest to small aspect ratios (delta wings) already separates at low angles of attack and leads to the formation of large-scale leading-edge vortices (see Fig. 1a), which come along with attached and separated, laminar and turbulent shear layers [1]. These flow structures are of an unsteady character over a broad range of scales and comprise non-linear interaction [2]. The vortex-induced additional velocities result in a nonlinear increase in lift in comparison to attached flow and lead to high maximum angles of attack.

As a rule, for high angles of attack, the vortex system is subject to a structural change:

the breakdown of the leading-edge vortex [3]-[5]. As a result of high circumferential velocities, high radial pressure gradients as well as low total pressures at the location of the vortex axis, the vortex comes to a critical state. The strongly increasing axial pressure gradient at the trailing edge then causes the reformation of the vortex core profiles from axially accelerated to decelerated flow in conjunction with a strong radial expansion of the vortex core (Fig. 1b). At Reynolds numbers and ratios of vortex-induced to free-stream velocities, which are typical for aerodynamic applications, the vortex bursting is of a spiral type [6]. The burst core flow is characterized by an instability type referred to as helical mode instability [4], [7].

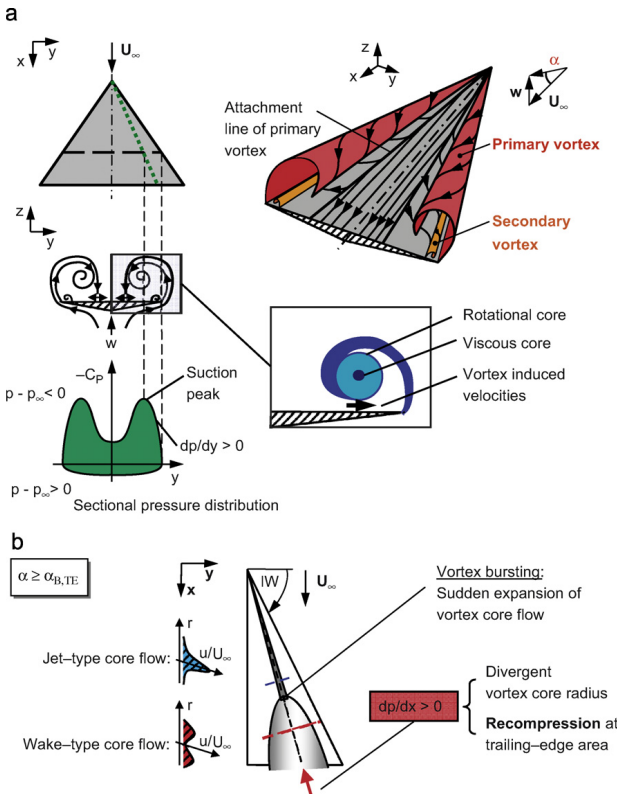

Fig. 1: Delta wing vortex formation: main delta wing flow features (a) and vortex bursting characteristics (b) [8].

The manipulation of the characteristic vortex flow instabilities is of great interest due to the possibility of increasing the performance of such configurations as well as the stability at the borders of the flight envelope, i.e. the control of the reattachment line and the breakdown location [5], [9]. This can be achieved by influencing the instabilities in the shear layer which rolls up to form the leading-edge vortex on the one hand and the flow state which leads to vortex bursting on the other hand.

One can distinguish between active and passive methods for the manipulation of leading-edge vortex structures. A passive means for flow control is for example the creation of multiple-vortex systems, such as those used with double delta wings or with the combination of main wing and strakes. Another method is the consciously generated interaction of structural oscillations of an elastic wing with the shear layer instabilities as presented in Ref. [9]. This supports the reattachment of the flow and leads to an increase in lift, but for transfer into practice, it has the disadvantage of additional dynamic loads on the wing structure.

The active means for flow control can be divided into three groups: control surfaces [9], continuous or periodic blowing or suction [10]-[13], and plasma actuators [14]. Control surfaces are for example leading-edge flaps for varying the angle of attack at the separation line, flaps for varying the leading-edge sweep, and flaps integrated at the apex of the wing. In the field of manipulation by pneumatic devices, continuous blowing and/or suction in the leading-edge region was investigated by Wood and Roberts [12], as well as concentrated tangential blowing in the apex region [9].

Except for the type of flow control, all means for manipulation can be classified into steady and unsteady methods. Both periodic blowing and the oscillation of flaps with small a deflection angle are more effective than their quasi-static counterparts [9]. The unsteady methods can be classified into low-frequency ($f\,c_r/U_\infty \approx 0.1$) and high-frequency ($f\,c_r/U_\infty \approx 1$) excitation. While low-frequency types can influence the burst behavior via variation of the axial pressure gradient, the high-frequency types aim at a manipulation of vortex-related instabilities.

However, an open issue in flow control mechanisms of leading-edge vortices is the extension of the angle of attack regime with attached flow by frequency-conditioned manipulation of the shear layer separation. This applies analogously to a fixation of the primary separation for rounded leading edges and the

attenuation of unsteady effects caused by the vortex breakdown. This issue could be addressed by periodic forcing, which takes the wave propagation characteristics of leading-edge vortices into account.

Therefore, the following presents a study conducted in the framework of a project funded by the German Research Association of the effect of periodic oscillations of sectional, active flap elements as well as of pulsed blowing using actuators integrated along the leading edge. This setup enables a specific intervention in the primary vortex shear layer by adjusting frequency and phase between the actuation segments along the leading-edge geometry. In this paper, we present the first experimental results of pulsed blowing.

2 Experimental Setup

2.1 Wind Tunnel Facilities

Experiments are conducted in the low speed wind tunnel facilities of the Institute of Aerodynamics and Fluid Mechanics of Technische Universität München (here: wind tunnel B; open test section with dimensions 1.2 m × 1.55 m × 2.8 m, $Tu_x \leq 0.4$ %) at a free stream velocity of $U_\infty = 24$ m/s ($Re_{mac} = 1.0 \times 10^6$).

2.2 Wind Tunnel Model

For all investigations, generic delta wing models representing the geometry of the Vortex Flow Experiment 2 configuration (VFE-2) will be used [15]. Within the VFE-2 project, an extensive numerical and experimental database on the flow around this wing configuration was gained [16]-[19]. It covers the cases of the partly developed, fully developed and the burst leading-edge vortex depending on the type of primary separation and the angle of attack. The data contains information in particular on the development of the boundary layer and spectral distributions of the turbulent fluctuations of the flow, which will be useful for the intention of flow manipulation.

The delta wing models have a wing sweep of $\varphi = 65°$ and a sharp leading-edge contour. The technical devices for flow manipulation will be integrated in the leading-edges.

The wind tunnel model equipped with a pulsed blowing system along the leading edge is a half-wing model with VFE-2 geometry. It has a root chord of $c_r = 0.98$ m, a wing half span of $s = 0.457$ m, a thickness of $\delta = 0.033$ m, and an aspect ratio of $\Lambda = 1.865$ (see Fig. 2).

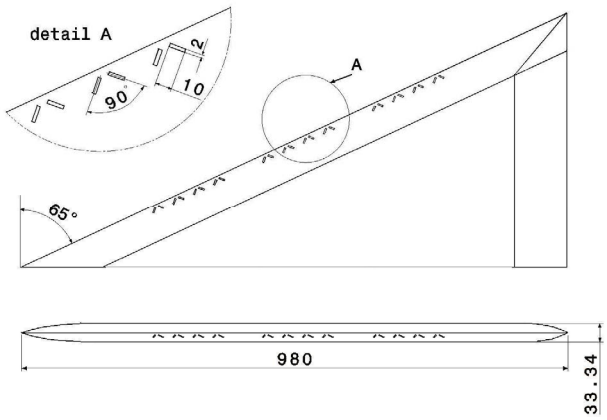

Fig. 2: Delta wing model with integrated leading-edge blowing sections

The model consists of metal plates (aluminum) for the wing surface and a leading-edge made of glass fiber composites, as well as a trailing edge of foamed plastic. The leading edge was produced in a counterpart mould construction.

The model is equipped with a péniche with a height of 55 mm (Fig. 3) to elevate the model out of the boundary layer of the balance table, minimizing the corresponding interference effects.

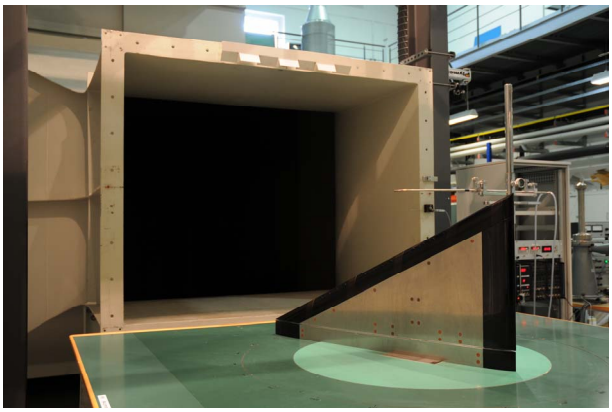

Fig. 3: Half model with péniche mounted in low-speed wind tunnel

The installed blowing system consists of three leading-edge sections which comprise a total of

twelve pairs of slots (size *t = 2 mm x h = 10 mm*) regularly distributed along the leading edge (Fig. 2). They are arranged slantwise to the leading edge with an orthogonal angle between the slots of each pair.

The compressed-air supply is provided in the form of the Institute's pressure line, which is connected via a tube system. The passage between the tubes and each pair of slots is realized by pre-chambers, which redirect the flow to the upper side of the leading edge and expand the jet to the slot size.

Electromagnetic valves are integrated between the tubes and the chambers. These generate the jet pulse. The valves switch between an opened and a closed state at a frequency of up to 1000 Hz. This pulse frequency can be controlled and varied over all 12 pairs of slots. Via synchronization of the 12 channels, the pulse phasing between the different valves can be adjusted.

The direction of the jet flow is approximately orthogonal to the wing surface. The jet velocity depends on the static pressure in front of the valves (in a closed state) and can be regulated. As the three leading-edge sections have individual pressure supplies, the velocity can be varied over the sections. In addition to the pulse frequency and the jet velocity, the duty cycle of the blowing (time ratio of the opened to the closed state of the valve) can be adjusted. The time series in Fig. 4 show the jet velocities measured 6 mm vertically over the slot at a duty cycle of *DC = 25%*. The average value of the velocity flank is 55 m/s. The pulse frequency can be inspected by a spectral analysis of the jet velocity signal (Fig. 5), which confirms the chosen frequencies. Furthermore, spectral peaks at higher harmonic frequencies can be detected.

In summary, the following parameters can be adjusted for unsteady blowing: the jet velocity at the three sections via pressure at the valves, the pulse frequency and the phasing, and the duty cycle of the jet at all 12 slot pairs. This offers a great variety of possible parameter combinations for the blowing setup. Therefore, particular attention should be paid to the choice of these parameters to succeed in vortex manipulation.

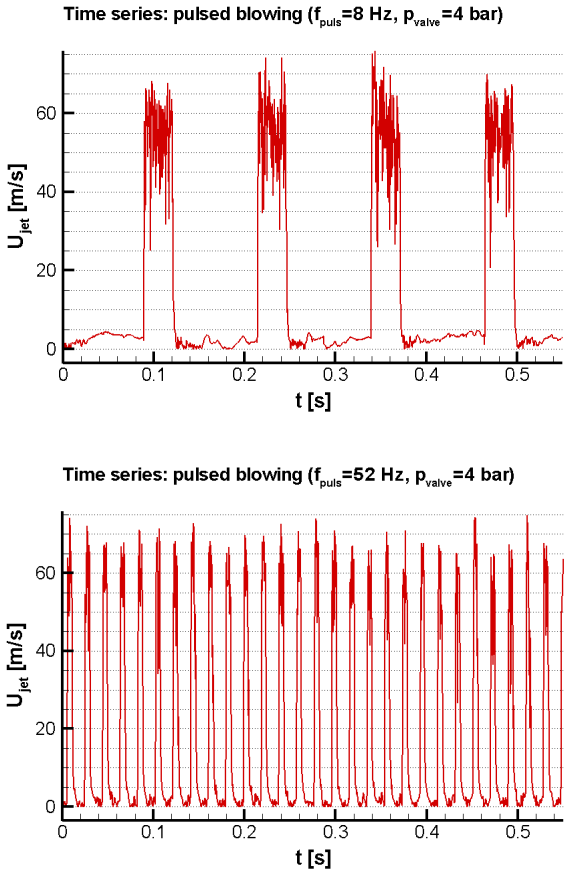

Fig. 4: Time series of jet velocity U_{jet} 6 mm over slot for f_{pulse} = 8 Hz and 52 Hz, DC = 25%, p_{valve} = 4 bar

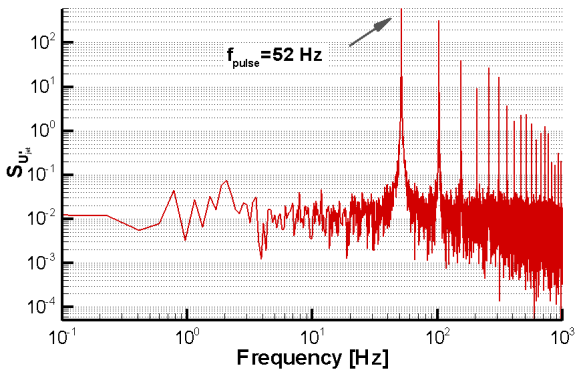

Fig. 5: Power spectral density of jet velocity for f_{pulse} = 52 Hz, DC = 25%, p_{valve} = 4 bar

2.3 Hot-Wire Anemometry

For all cases, flow field measurements applying advanced hot-wire anemometry (HWA) are conducted which allow the flow topology, the mean velocity field, turbulence intensities, and spectral quantities to be analyzed. The measurements are carried out with crosswire-

type miniature probes on the basis of a look-up table technique for constant temperature anemometry (CTA) and include a temperature correction. A sampling rate of 3000 Hz is used in combination with a low-pass filter of 1400 Hz. For each point, a number of 19,200 samples is recorded.

During one measurement cycle, two velocity components can be observed: the axial component u and one orthogonal component (v or w). To gain the third velocity component, the measurement has to be repeated with the probe rotated about 90° in the axial direction.

The measurement planes are located at chord-wise positions $x_b/c_r = 0.4$, 0.6 and 0.8 with a grid resolution of $\Delta = s_l/20$ in the spanwise and vertical directions (Fig. 6).

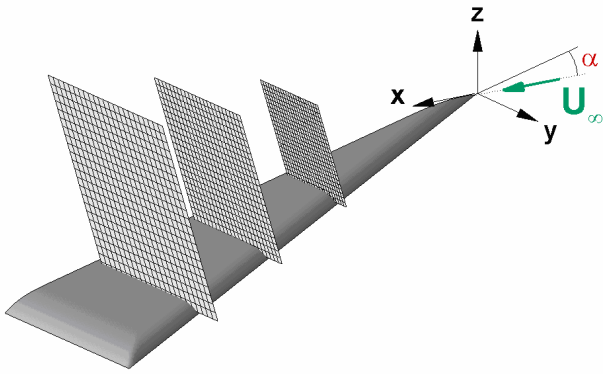

Fig. 6: Cross-flow planes of HWA measurements at stations x_b/c_r = 0.4, 0.6 and 0.8 on the half-wing model

3 Actuation Strategy

The parameter set for the flow actuation is chosen on the basis of the flow physics associated with the delta wing model as well as on the present findings in the manipulation of delta wing vortex systems.

3.1 Frequencies (Instabilities)

The actuators will be run in the frequency range of the inherent instability types for free-stream velocities of $U_\infty = 24$ m/s. In theory, these are for the half wing model with VFE-2 geometry:

- the frequency range for excitation at the subharmonic f_A of the shear layer instabilities f_S [11], [20]:

$$f_S = \frac{U_\infty (2000 \div 10000)}{c_r \sqrt{\mathrm{Re}_{c_r}}} \approx 40 \div 200\, Hz \qquad (1)$$

$$f_A = (0.25 \div 0.5) f_S \approx 10 \div 100\, Hz, \qquad (2)$$

- the range for excitation at the frequency of the helical mode instability f_{dom} associated with vortex bursting [8]:

$$f_{dom} = \frac{1}{c_r \cot\varphi} \cdot \frac{U_\infty}{\sin\alpha} \cdot (0.28 \pm 0.025), \qquad (3)$$

which depends on the local chord coordinate and has different values for the three measurement planes:

$$f_{dom} \approx \begin{cases} 85 \div 105\, Hz & for\ x_b/c_r = 0.4, \\ 57 \div 68\, Hz & for\ x_b/c_r = 0.6, \\ 43 \div 52\, Hz & for\ x_b/c_r = 0.8, \end{cases}$$

- and the range for excitation at the frequency f_B, related to the quasi-periodic fluctuations of the vortex breakdown location [9]:

$$f_B = (0.05 \div 0.1) \frac{U_\infty}{l_\mu} \approx 1.8 \div 3.7\, Hz. \qquad (4)$$

3.2 Choice of Actuation Parameters

Pulse frequency and phasing

The starting point for the choice of the pulse frequencies is an analysis of the flow field without actuation at $\alpha = 23°$ and $U_\infty = 24$ m/s ($Re = 1 \cdot 10^6$), which corresponds to the case of vortex bursting over the delta wing at $x_b/c_r \approx 0.3$. Therefore, HWA measurements in the three presented planes (see Fig. 6) are carried out without blowing (the results of these measurements are discussed in more detail in Sec. 4.1). In the next step, the power spectral density of the measured velocity components is analyzed at certain points of largest inflection in the radial profiles of retarded axial core flow to identify the frequencies of the instability types for the burst vortex. At this point, special attention will be paid to the helical mode instability of vortex bursting.

Fig. 7 shows a contour plot of the axial turbulence intensity for $\alpha = 23°$ in the rear

measurement plane at $x_b/c_r = 0.8$. It clearly reveals the annular structure of the burst vortex core [20]. The spectral analysis in this region (chosen for the position marked in Fig. 7) shows a narrow-band concentration of turbulent kinetic energy in the frequency range of 55 to 76 Hz. This spectral density peak is linked to the helical mode instability of vortex bursting. Its values do not match exactly those given by Eq. 3, but are close to the expected region.

In the spectral analysis for the annular structure of the vortex core, several "needles" were detected at single values of $f = 65$ Hz and $f = 76$ Hz. For the second measurement plane $(x_b/c_r = 0.6)$, the concentration of kinetic energy is measured at $f = 65$ Hz to $f = 103$ Hz.

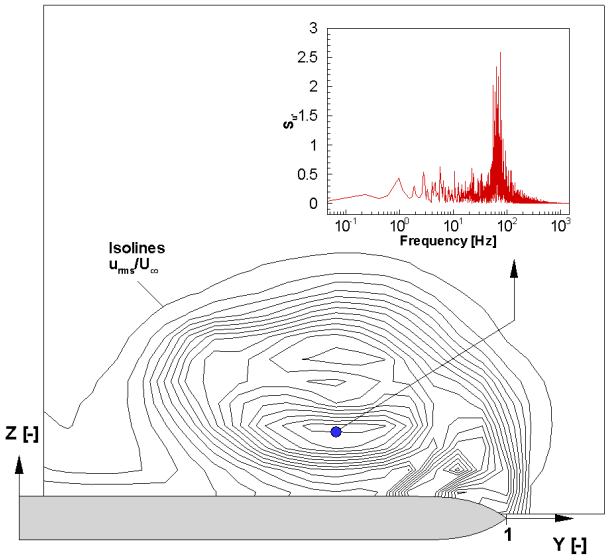

Fig. 7: Power spectral density for fluctuations of axial velocity component (S_u') for burst vortex at $\alpha = 23°$, $x_b/c_r = 0.8$, $Re_{mac} = 1 \cdot 10^6$ and M = 0.07 (w/o actuation)

The frequencies chosen on the basis of the spectral analysis are $f_{pulse} = 4,\ 52,\ 65,\ 76,$ and 103 Hz. While the four higher frequencies lie in the range of the helical mode instability, $f_{pulse} = 4$ Hz could be representative for the quasi-periodic fluctuations of the vortex breakdown location. The value was chosen because different peaks were detected at this frequency in the spectral analysis. In the first investigations, the same pulse frequency was run over all slots without phase displacement. The chosen duty cycle is $DC = 25\%$.

Jet velocity

In Ref. 11, Gad-el-Hak and Blackwelder applied periodic blowing and suction through slots along both leading edges to a 60° delta wing. They varied the peak ejection and suction speeds from 0 to 2 times the freestream velocities. The momentum coefficients were in the range of $C_\mu = 1x10^{-4} \div 6x10^{-4}$. Gu et al., who examined tangential blowing and suction along the leading edge of a 75° half-delta wing [13], gained the best results with a momentum coefficient of $C_\mu = 3.6x10^{-2}$.

In the present case the momentum coefficient related to one slot can be estimated as follows:

$$C_\mu = \frac{\dot{m}_{jet} U_{jet}}{\frac{\rho_\infty}{2} U_\infty^2 F} = 2\left(\frac{U_{jet}}{U_\infty}\right)^2 \frac{th}{\frac{1}{4} c_r b} \qquad (5)$$

with the assumptions of a constant blowing profile over the slot, $\rho_{jet} \approx \rho_\infty$, $F_{slot} = t \cdot h$ and the wing surface $F = c_r b/4$. For the investigations reported here, a jet velocity of $U_{jet} = 55$ m/s was used, which corresponds to 2.3 times the freestream velocity resulting in a momentum coefficient of $C_\mu = 9.4x10^{-4}$.

4 Results and Discussion

The results of HWA measurements at a free-stream velocity of $U_\infty = 24$ m/s and an angle of attack of $\alpha = 23°$ are presented for the baseline and one controlled case. In the actuated case, sectional blowing with $f_{pulse} = 65$ Hz, $DC = 25\%$ and $U_{jet} = 55$ m/s is carried out.

4.1 Mean and Turbulent Flowfield

Figs. 8–11 show the time averaged axial and vertical velocity components u and w as well as their corresponding fluctuation intensities u_{rms} and w_{rms} for the two studied cases. Furthermore, for easier evaluation of the control effect, they display the difference between these values (difference between the actuated and the non-actuated cases).

Baseline case

A fully developed leading-edge vortex is fed by the shear layer which is shed along the entire leading edge of the delta wing at moderate angles of attack, rolling up to form the rotational core of the primary vortices (see Fig. 1a). This rotational core contains an embedded sub-core, which is dominated by viscous effects and characterized by high axial velocities as well as low static pressures. The high gradients involved in the cross-flow velocities cause enhanced velocity fluctuations, which are concentrated in the viscous sub-core of the primary vortex in form of a circle-like region of local rms maxima. The highly increased mean velocities on the upper wing surface coincide with high suction peaks, which lead to additional lift for wings with a stable, fully developed leading-edge vortex system. For sharp leading-edge contours, the position and the strength of the vortex system mainly depends on the angle of attack.

The change in the vortex core structure referred to as the vortex breakdown (see Sec. 1) occurs at further increasing angles of attack. It is characterized by the transition from stable to unstable core flow, which leads to a sudden expansion of the vortex core. The breakdown position moves in the direction of the apex with increasing angle of attack. The vortex core expansion is reflected by strongly decelerated axial flow as well as an annular structure of local rms maxima of the axial velocity component in the cross-flow sections of the burst vortex.

For the uncontrolled or baseline case measured at $\alpha = 23°$, the vortex breakdown already progresses from the rear part of the wing to $x_b/c_r \approx 0.3$. This is clearly depicted by the annular structure of local rms maxima of the axial velocity in the cross sections at $x_b/c_r = 0.4$ and $x_b/c_r = 0.6$ (Fig. 8 & Fig. 10, top right) which are at a very high level ($u_{rms}/U_\infty = 0.38$). Also, the secondary vortex is marked by a local maximum of turbulence intensity near the leading edge.

Another sign for the burst vortex is the area of retarded axial flow ($u = 13$ *m/s*) in both measurement planes (top left of both figures). The axial core velocity is considerably below the value of the free stream velocity ($U_\infty = 24$ *m/s*) and the corresponding area expands in a chordwise direction.

The vertical velocity pattern is characterized by an upward field which originates from the acceleration of the flow from the lower wing side to the upper wing side around the leading edge as well as from the upward component of the primary vortex. The downward velocities of the vortex form the corresponding downward field on the opposite side. The intensity of both zones decreases in a chordwise direction (see Fig. 9 & Fig. 11, top left).

Controlled case

For the controlled case with pulsed blowing at 65 Hz, the annular structure of axial turbulence intensity, which is a criterion for burst vortices, does not exist anymore in the first cross section at station $x_b/c_r = 0.4$ (Fig. 8). It is replaced by a circular structure, which is typical for fully developed vortices. Furthermore, the region of retarded axial flow between the two local maxima is eliminated, which results in high differences in the axial velocity component between the controlled and the uncontrolled case ($\Delta u_{max} = 17$ *m/s*). The axial peak velocity on the wing surface is slightly increased from $u/U_\infty = 2.3$ to $u/U_\infty = 2.4$. Also, the isolines of the vertical velocity component at station $x_b/c_r = 0.4$ are situated closer to each other at the central crossover from the upward to the downward velocities, which results from an expansion of both regions. The maximum of the vertical turbulence intensities is remarkably increased for the controlled case.

In the second crossflow plane at station $x_b/c_r = 0.6$ (Figs. 10−11), fewer differences are noticed between the controlled and the uncontrolled case. The criteria for a burst vortex are fulfilled (annular structure of rms maxima, region of retarded axial flow), but the levels of the retarded axial velocity and the maximum axial turbulence intensity in the region of the annular structure are slightly reduced.

In conclusion, the breakdown location is displaced downstream by pulsed blowing at $f_{pulse} = 65$ *Hz* when compared to the uncontrolled case.

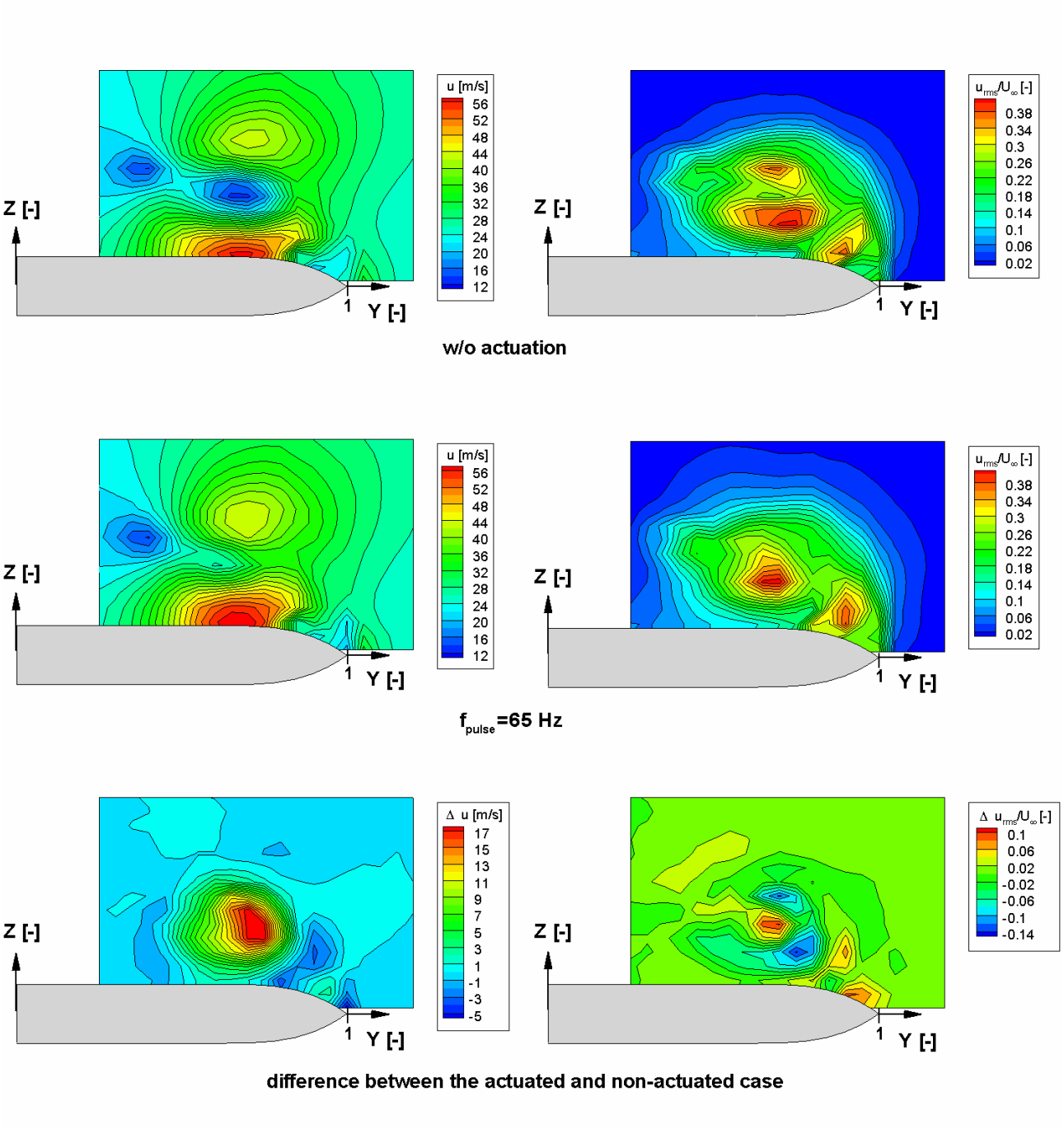

Fig. 8: Mean and turbulent axial velocity fields for the non-actuated and actuated cases at $\alpha = 23°$, $x_b/c_r = 0.4$, $Re_{mac} = 1 \cdot 10^6$, and $M = 0.07$; $f_{pulse} = 65$ Hz

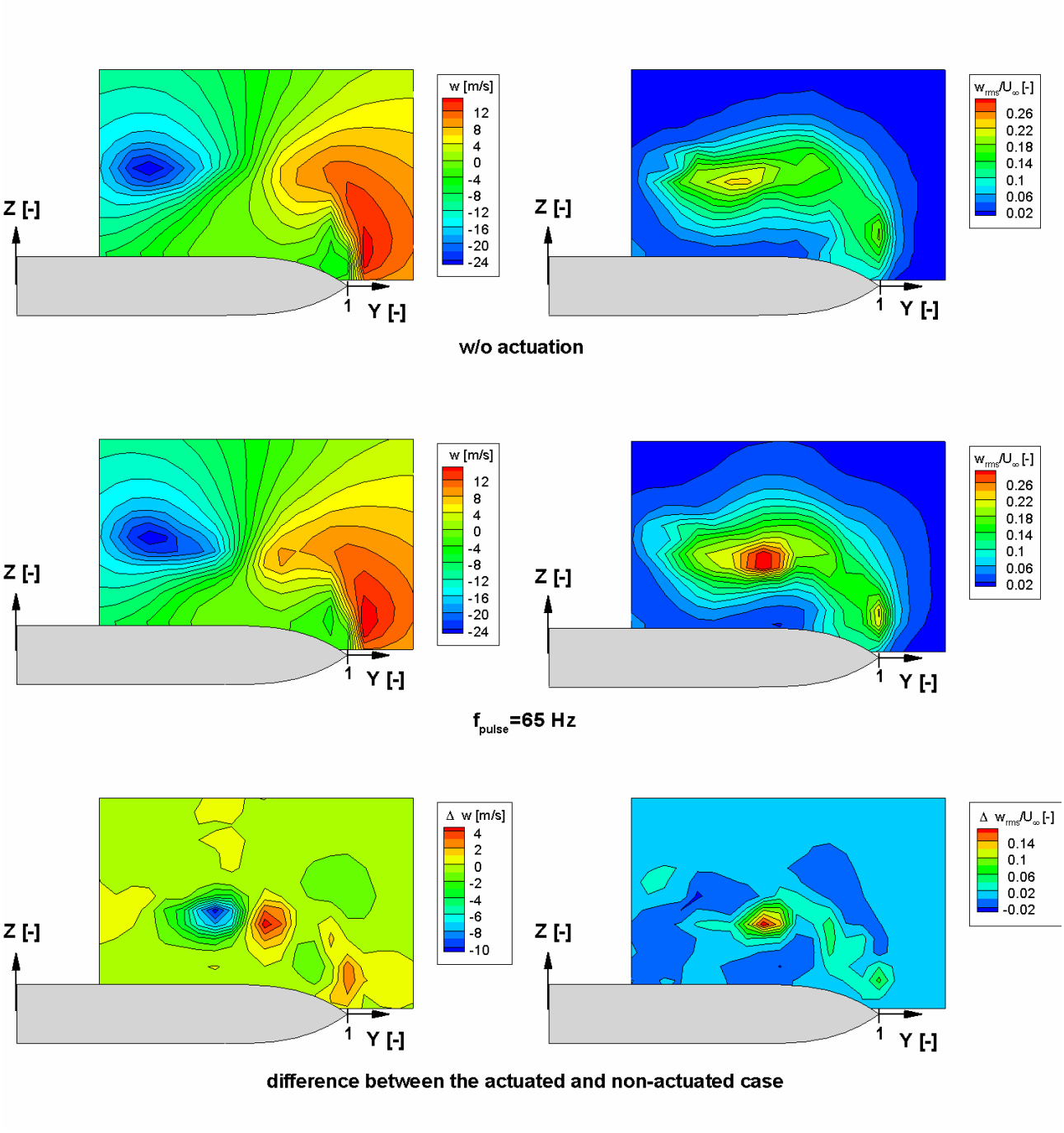

Fig. 9: Mean and turbulent vertical velocity fields for the non-actuated and actuated cases at $\alpha = 23°$, $x_b/c_r = 0.4$, $Re_{mac} = 1 \cdot 10^6$, and $M = 0.07$; $f_{pulse} = 65$ Hz

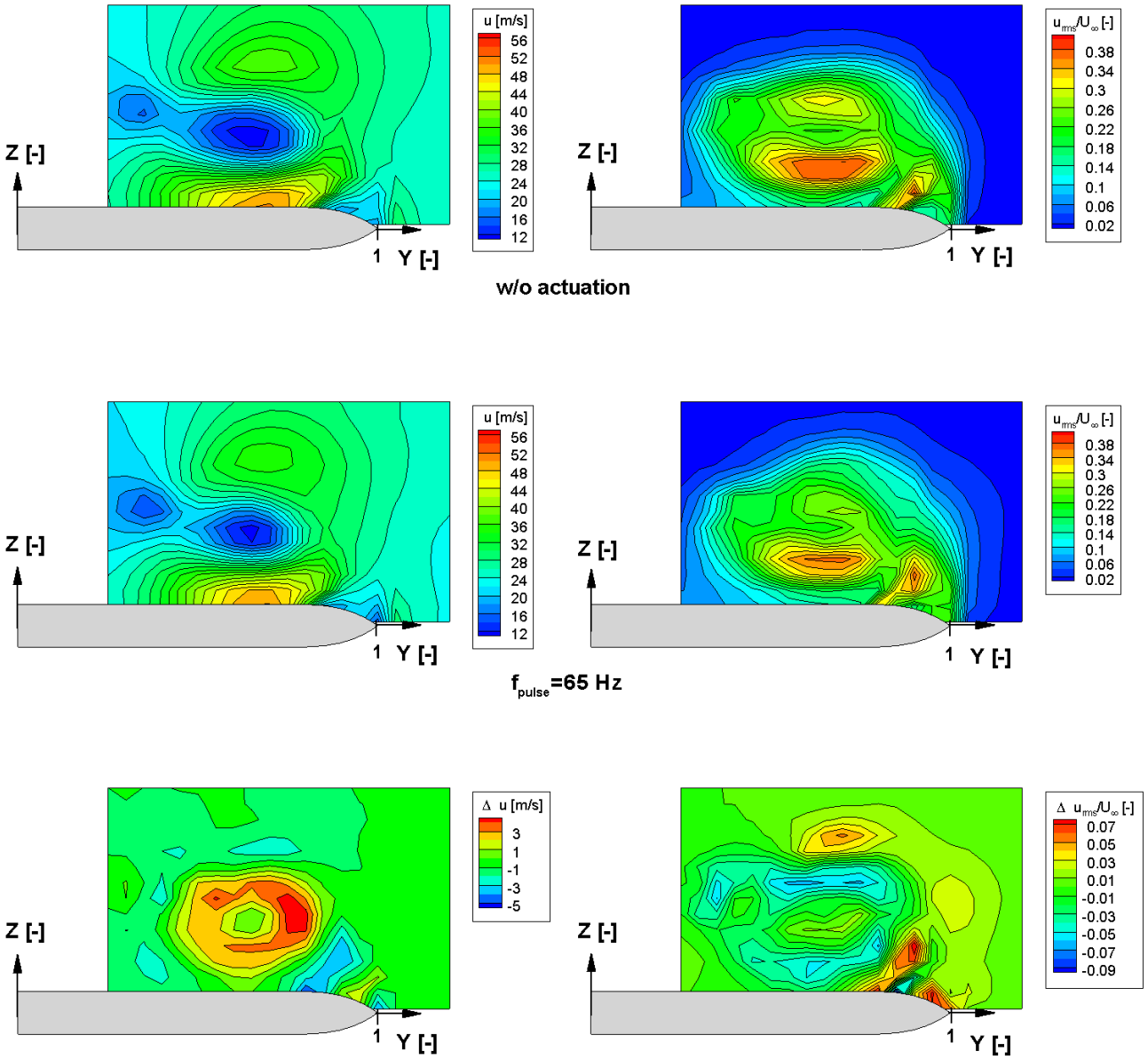

Fig. 10: Mean and turbulent axial velocity fields for the non-actuated and actuated cases at $\alpha = 23°$, $x_b/c_r = 0.6$, $Re_{mac} = 1 \cdot 10^6$, and $M = 0.07$; $f_{pulse} = 65$ Hz

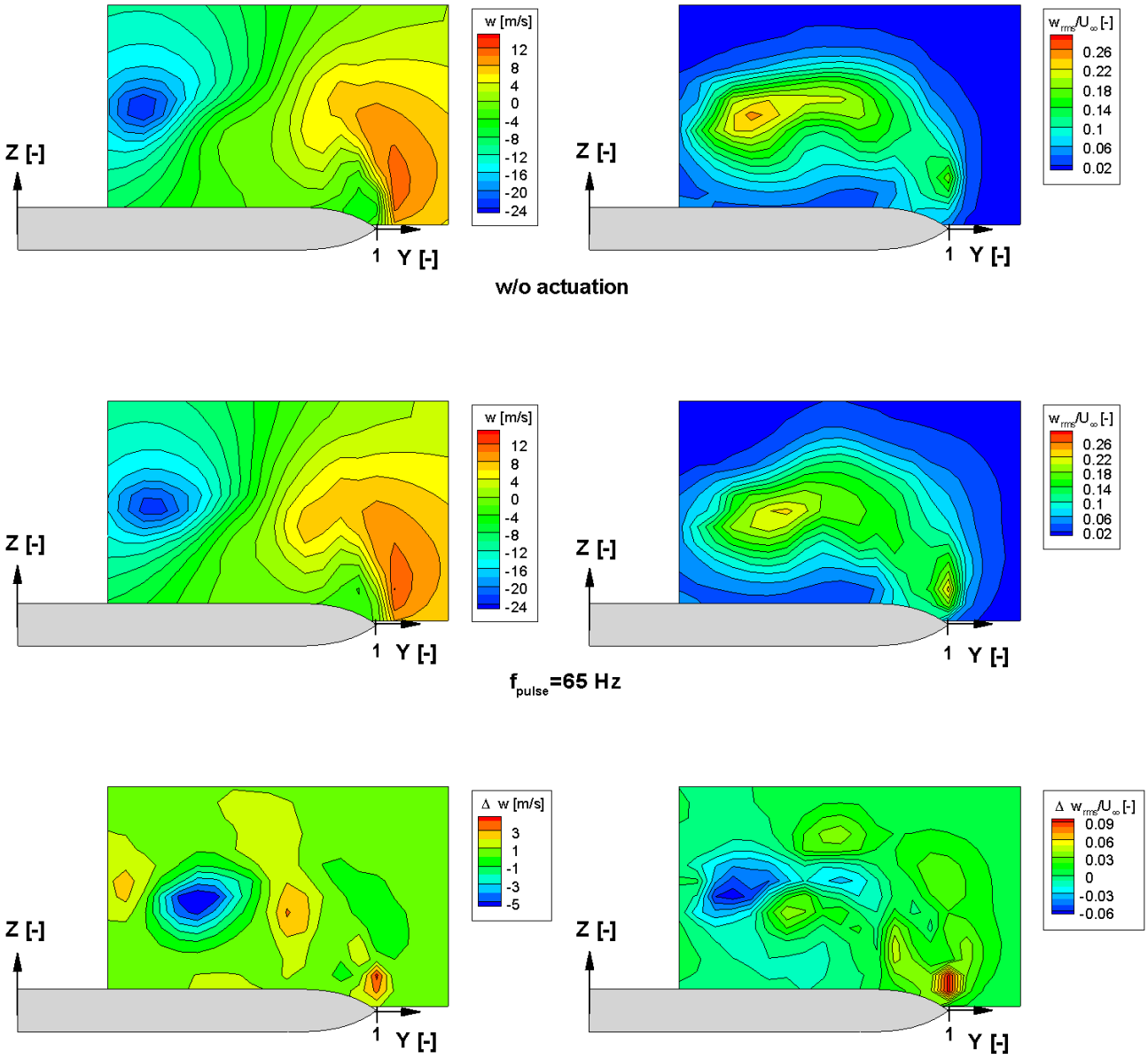

Fig. 11: Mean and turbulent vertical velocity fields for non-actuated and actuated case at $\alpha = 23°$, $x_b/c_r = 0.6$, $Re_{mac} = 1 \cdot 10^6$, and $M = 0.07$; $f_{pulse} = 65$ Hz

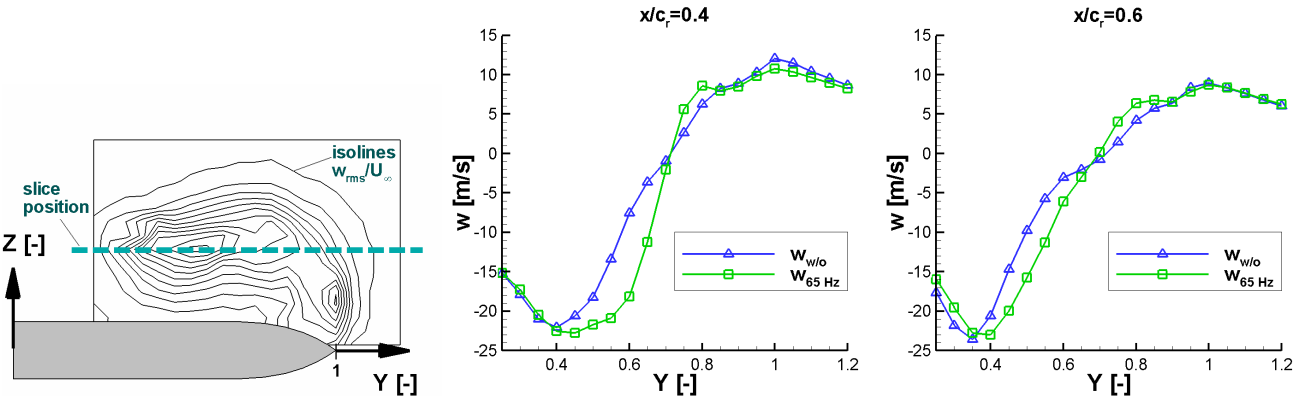

Fig. 12: Vertical velocity component in horizontal slices through the vertical position of the vortex center at α = 23°, x_b/c_r = 0.4 / 0.6, Re_{mac} = 1•10^6, and M = 0.07

In Fig. 12, two plots of the vertical velocity component are shown for both the actuated and the non-actuated case for a horizontal slice through the vortex center, which corresponds to the position of the maximum w_{rms} value (left plot). The gradient of the vertical velocity component is measurably increased by pulsed blowing, especially in the first measurement plane at $x_b/c_r = 0.4$. This trend visualizes the concentration of the vortex by means of pulsed blowing in the chosen frequency.

4.2 Spectral Analysis

At this point, the axial velocity spectra at different locations of the leading-edge vortex in the cross section at station $x_b/c_r = 0.8$ are compared for the non-actuated and the actuated case (see Figs. 13−14).

For measurement point 3 of the non-actuated case, which is situated in the outer shear layer region, the u_{rms} value is remarkably higher than in the area not affected by the leading-edge vortex. A moderate increase of turbulent kinetic energy in a very broad frequency range from 80 to 400 Hz is registered at this point. In the shear layer over the burst vortex core at measurement point 2, these amplitude peaks are slightly higher, but with a steep decline to higher frequencies. The highest values of turbulent kinetic energy appear at a point in the annular core region as a narrow-band concentration at a frequency of approximately 55 to 76 Hz, which is linked to the helical mode instability of vortex bursting (see also Sec. 3.2).

For the actuated case, the spectra of all measurement points show very high amplitude peaks at the pulse frequency and corresponding higher harmonic frequencies, respectively. The detected values of power spectral density at the pulse frequencies are approximately one order of magnitude higher than the values of the baseline case. This verifies the receptivity of the shear layer for pulsed blowing. Besides these dominant peaks, the spectral characteristics for measurement points 2 and 3 are quite similar to these of the uncontrolled ones. This is not the case for measurement point 1 in the core: The spectrum reveals the former concentration of kinetic energy at the narrow frequency band neither at this point nor at other measurement stations of the core region.

Here, a high-frequency excitation has been studied applying pulsed blowing. Unsteady momentum is added near the separation line in the frequency range of the helical mode instability associated with vortex bursting. Small scale vortical structures shed at the actuator slots influence the shear layer forming the rotational core of the leading-edge vortex. The periodicity fed to the shear layer stabilizes the fully developed part of the leading-edge vortex the evolution of which is close to breakdown. These findings substantiate that flow control applying high-frequency excitation can effectively influence a leading-edge

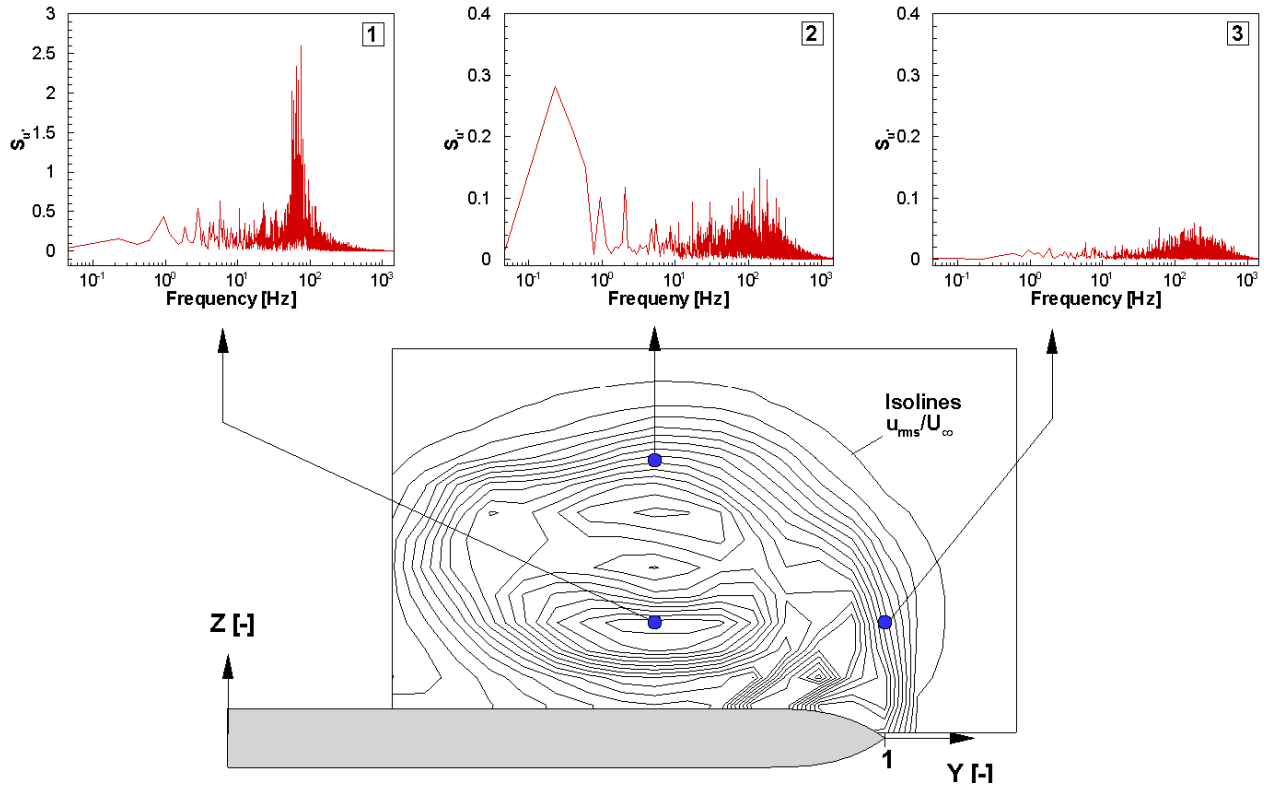

Fig. 13: Power spectral densities for axial velocity fluctuations ($S_{u'}$) in the shear layer and the burst vortex core at $\alpha = 23°$, $x_b/c_r = 0.8$, $Re_{mac} = 1 \cdot 10^6$, and $M = 0.07$ (w/o actuation)

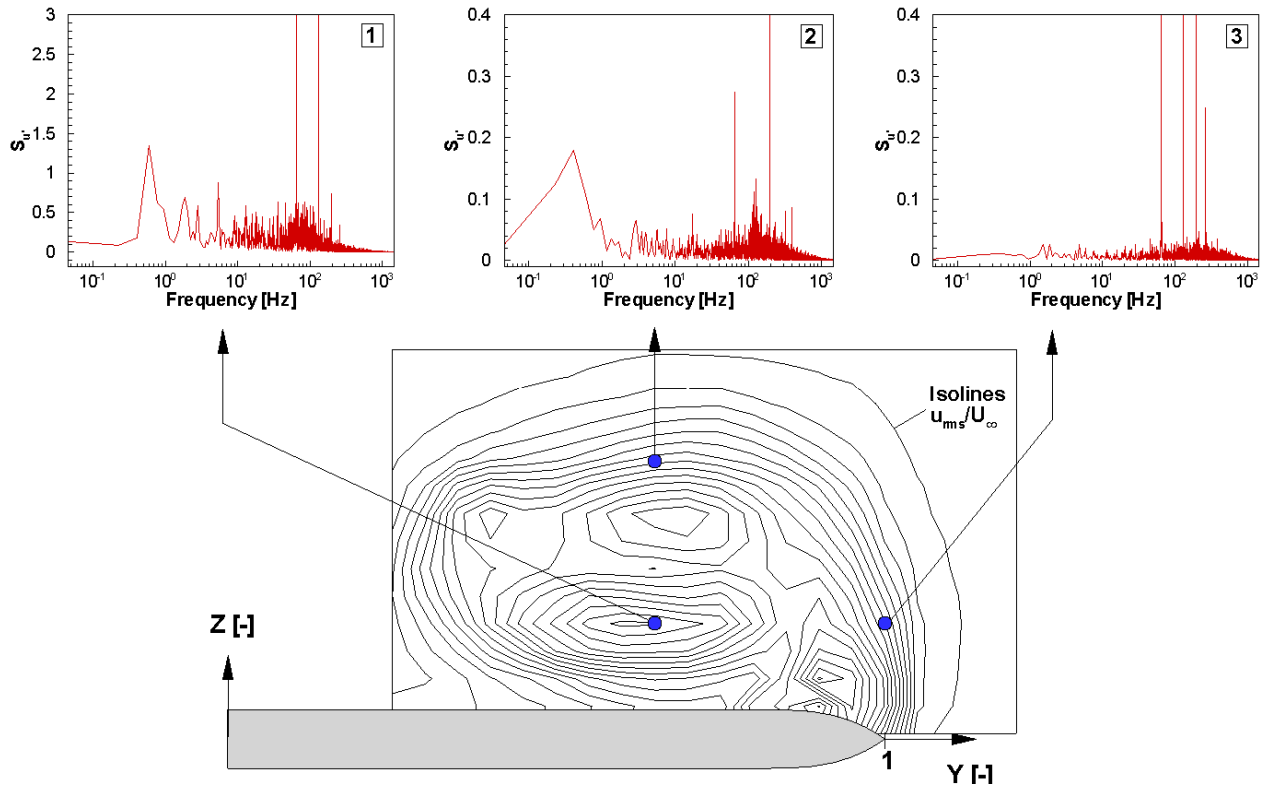

Fig. 14: Power spectral densities for axial velocity fluctuations ($S_{u'}$) in the shear layer and the burst vortex core at $\alpha = 23°$, $x_b/c_r = 0.8$, $Re_{mac} = 1 \cdot 10^6$, and $M = 0.07$ ($f_{pulse} = 65$ Hz)

vortex, consisting of an upstream fully developed part, and a downstream breakdown region. Compared to the case without excitation the vortex breakdown station is shifted downstream, thus extending the upstream, high energy part of the vortex. Consequently, the downstream shift of vortex bursting results in an increase in lift and a reduction of unsteady loads.

5 Summary and Outlook

Experimental investigations on pulsed blowing along the leading edge of a delta half wing model were carried out to evaluate the effect on the aerodynamic performance of delta wings. The choice of the pulse frequency is based on a spectral analysis of the flow to assess its inherent instabilities.

The results of hot-wire field measurements prove the receptivity of the shear layer for actuation at the chosen frequency, which is clearly detectable in the spectral analysis of the axial velocity component along the whole vortex structure. The manipulation of the vortex system at the frequency of the helical mode instability of vortex bursting leads to a displacement of the vortex breakdown location in a chordwise direction. In regard to the aerodynamic performance of such configurations, this is a strongly desired effect. Force and pressure measurements will be conducted to further evaluate the impact of vortex manipulation on the aerodynamic characteristics.

Moreover, further parametric investigations of blowing velocity and frequencies will be carried out. The authors also intend to adapt the frequencies of pulsed blowing along the leading edge to address the variation of instability frequencies in a chordwise direction. Considering the phenomenon of wave propagation, the application of a phase displacement along the leading edge to pulsed blowing will be tested.

References

[1] Hummel, D.: On the Vortex Formation over a Slender Wing at Large Angles of Incidence, *High Angle of Attack Aerodynamics*, AGARD-CP-247, pp.15-1−15-17, Sandfjord, Norway, 1978.

[2] Gad-el-Hak, M., and Blackwelder, R.F.: The Discrete Vortices from a Delta Wing, *AIAA Journal*, Vol. 25, No. 8, pp. 1042−1049, 1987.

[3] Hummel, D.; Documentation of Separated Flows for Computational Fluid Dynamics Validation, *Validation of Computational Fluid Dynamics*, Vol. 2, AGARD-CP-437, pp. 18-1−18-24, Lisbon, Portugal, May 1988

[4] Gursul, I.: Unsteady Flow Phenomena over Delta Wings at High Angle of Attack, *AIAA Journal*, Vol. 32, No. 2, pp. 225−231, 1994.

[5] Mitchell, A. M., and Delery, J.: Research into Vortex Breakdown Control, *Progress in Aerospace Sciences*, Vol. 37, pp. 385-418, 2001.

[6] Müller, J., and Hummel, D.: Time-Accurate CFD-Analysis of the Unsteady Flow on a Fixed Delta Wing, *AIAA Paper* 2000-0138, 2000.

[7] Gursul, I., Gordinier, R., and Visbal, M.: Unsteady Aerodynamics of Nonslender Delta Wings, Progess in Aerospace Sciences, Vol. 41, pp. 515−557, 2005.

[8] Breitsamter, C.: Unsteady Flow Phenomena Associated with Leading-Edge Vortices. *Progress in Aerospace Science,* Vol. 44, pp. 48-65, 2008.

[9] Gursul, I., Wang, I., and Vardaki, E.: Review of Flow Control mechanisms of Leading-edge Vortices. *Progress in Aerospace Science,* Vol. 43, pp. 246−270, 2007.

[10] Greenblatt, D., and Wygnanski, I. J.: The Control of Flow Separation by Periodic Excitation. *Progress in Aerospace Science,* Vol. 36, pp. 487−545, 2000.

[11] Gad-el-Hak, M., and Blackwelder, R. F.: Control of the Discrete Vortices from a Delta Wing, *AIAA Journal*, Vol. 25, No. 8, pp. 1042−1049, 1987.

[12] Wood, N. J., and Roberts, L.: Control of Vortical Lift on Delta Wings by Tangential Leading-Edge Blowing, *Journal of Aircraft*, Vol. 25, No. 3, pp. 236−243, 1988.

[13] Rockwell, D., Gu, W., and Robinson, O.: Control of Vortices on a Delta Wing by Leading-Edge Injection, *AIAA Journal*, Vol 31.7, pp. 1177−1186 , 1993.

[14] Greenblatt, D., Kastantin, Y., Nayeri, C. N., and Paschereit, C. O.: Delta-Wing Flow Control Using Dielectric Barrier Discharge Actuators, *AIAA Journal*, Vol. 46, No. 6, pp. 1554−1560, 2008.

[15] Chu, J., and Luckring, J. M., Experimental Surface Pressure Data Obtained on 65 deg Delta Wing across Reynolds Number and Mach Number Ranges, *NASA-TM-4645*, 1996.

[16] Furman, A. and Breitsamter, C.: Turbulent and Unsteady Flow Characteristics of Delta Wing Vortex Systems. *46th AIAA Aerospace Sciences Meeting and Exhibit*, Reno, Nevada, 2008.

[17] Furman, A. and Breitsamter, C.: Experimental Investigations on the VFE-2 Configuration at TU Munich, Germany, *Summary report of Task Group RTO-TR-AVT-11: Understanding and Modeling Vortical Flows to Improve the Technology Readiness Level for Military Aircraft*, ISBN 978-92-837-0073-9, 2009.

[18] Hummel, D.: Review of the Second International Vortex Flow Experiment (VFE-2), *AIAA Paper* 2008−377, Jan. 2008.

[19] Luckring, J. M., Hummel, D.: What was Learned from the VFE-2 Experiments? *AIAA Paper 2008-383*, 2008.

[20] Breitsamter, C.: *Turbulente Strömungsstrukturen an Flugzeugkonfigurationen mit Vorderkantenwirbeln*, Dissertation, Technische Universität München, Herbert Utz Verlag, ISBN 3-89675-201-4, 1997.

Acknowledgement

The authors would like to thank the German Research Association (Deutsche Forschungsgemeinschaft, DFG) for the funding of the project.

Copyright Statement